Biophysical Journal Volume 85 November 2003 3367–3374

Role of the Aromatic Ring of Tyr43 in Tetraheme Cytochrome c_3 from *Desulfovibrio vulgaris* Miyazaki F

Kiyoshi Ozawa,[†] Yuki Takayama,[*] Fumiko Yasukawa,[†] Tomoaki Ohmura,[‡] Michael A. Cusanovich,[§] Yusuke Tomimoto,[¶] Hideaki Ogata,[¶] Yoshiki Higuchi,[¶||] and Hideo Akutsu[* **]

[*]Institute for Protein Research, Osaka University, Suita, Japan; [†]Faculty of Engineering, Yokohama National University, Yokohama, Japan; [‡]Yokohama Research & Development Center, Mitsubishi Heavy Industries, Yokohama, Japan; [§]Department of Biochemistry, University of Arizona, Tucson, Arizona; [¶]Division of Chemistry, Graduate School of Science, Kyoto University, Kyoto, Japan; [||]RIKEN Harima Institute/SPring-8, Hyogo, Japan; and [**]Institute for Molecular Science, Okazaki National Institutes, Okazaki, Japan

ABSTRACT Tyrosine 43 is positioned parallel to the fifth heme axial ligand, His34, of heme 1 in the tetraheme cytochrome c_3. The replacement of tyrosine with leucine increased the redox potential of heme 1 by 44 and 35 mV at the first and last reduction steps, respectively; its effects on the other hemes are small. In contrast, the Y43F mutation hardly changed the potentials. It shows that the aromatic ring at this position contributes to lowering the redox potential of heme 1 locally, although this cannot be the major contribution to the extremely low redox potentials of cytochrome c_3. Furthermore, temperature-dependent line-width broadening in partially reduced samples established that the aromatic ring at position 43 participates in the control of the kinetics of intramolecular electron transfer. The rate of reduction of Y43L cytochrome c_3 by 5-deazariboflavin semiquinone under partially reduced conditions was significantly different from that of the wild type in the last stage of the reduction, supporting the involvement of Tyr43 in regulation of reduction kinetics. The mutation of Y43L, however, did not induce a significant change in the crystal structure.

INTRODUCTION

A variety of polyheme Class III *c*-type cytochromes (Ambler, 1980) from the sulfate-reducing bacteria have been isolated and characterized. Within the superfamily (Bruschi, 1994), examples include tetraheme cytochromes c_3 (cyt c_3; mol. wt. ~14,000; Coutinho and Xavier, 1994), octaheme cyt c_3 (mol. wt. ~26,000; Bruschi, 1994), and hexadecaheme cytochrome, Hmc (Pollock et al., 1991). The three dimensional structures of several tetraheme cyt c_3 have been determined (Harada et al., 2002 and references therein), as well as the structures of octaheme cyt c_3 (Czjzek et al., 1996) and Hmc (Matias et al., 2002; Czjzek et al., 2002). An important characteristic of cyt c_3 is the extremely low oxidation-reduction (redox) potential of the hemes, ranging from −165 to −400 mV as compared to ~260 mV for the mitochondrial Class I *c*-type cytochromes (Mathews, 1985). The low redox potential hemes, a consequence of bis-histidine ligation and the environment provided by the folded protein, facilitates the metabolic need for the *Desulfovibrio* to reduce the relatively weak oxidant, sulfate. In the course of studies designed to better understand the folding, redox properties and function of the cyt c_3, site-directed mutagenesis using an overexpression system from *Desulfovibrio desulfricans* has been effectively used (Dolla et al., 1994; Salgueiro et al., 2001). Nevertheless, much remains to be learned about the role of specific amino-acid side chains, in part because of limited amounts of mutated cytochrome. Recently, we have developed a novel overexpression system of multiheme cyt c_3 using the facultative anaerobe, *Shewanella oneidensis* (Ozawa et al., 2001). This system permits the production of relatively large amounts of cyt c_3 site-directed mutants and thus facilitates structural studies.

One of the important characteristics of cyt c_3 is the presence of aromatic rings in the vicinity of axial ligands of four hemes. The significance of these aromatic rings has been indicated in the literature from the structural point of view (Higuchi et al., 1984; Czjzek et al., 1994), although their individual roles are still not clear. Among the highly conserved aromatic residues, tyrosine 43 (Y43) is an interesting candidate for structural studies. It is present in *Desulfovibrio vulgaris* Miyazaki F (*Dv*MF), *D. vulgaris* Hildenborough (*Dv*H), *D. gigas* (*Dg*), and *D. desulfuricans* ATCC 27774 (*Dd*A) (Nørager et al., 1999), which commonly have the heme binding motifs CXXCH, CXXXXCH, CXXCH, and CXXXXCH from the amino to carboxyl termini (X is any amino acid). The aromatic ring of this tyrosine is parallel to the imidazole of histidine 34, the fifth axial ligand of heme 1 (the heme numbering according to the sequence) and in close proximity (within 4 Å). Note that the *Dv*MF cyt c_3 has one more alanine at the N-terminus (Ozawa et al., 2001) compared to the reported sequence (Kitamura et al.,

Submitted June 22, 2003, and accepted for publication July 23, 2003.

Address reprint requests to Hideo Akutsu, Osaka University, 3-2 Yamadaoka, Suita 565-0871, Japan. Tel.: 81-6-6879-8597; Fax: 81-6-6879-8599; E-mail: akutsu@protein.osaka-u.ac.jp.

Kiyoshi Ozawa's current address is the Research School of Chemistry, Australian National University, Canberra, ACT 0200, Australia.

Yoshiki Higuchi's current address is the Graduate School of Science, Himeji Institute of Technology, 3-2-1 Koto Kamigori, Hyogo 678-1297, Japan.

Abbreviations used: Tyr, tyrosine; Y43L, a mutation with Tyr43 replaced by leucine; NMR, nuclear magnetic resonance; 5-dRf, 5-deazariboflavin; *Dv*MF, *Desulfovibrio vulgaris* Miyazaki F; *Dv*H, *D. vulgaris* Hildenborough; *Dg*, *D. gigas*; *Dd*A, *D. desulfuricans* ATCC 27774; *Dd*E, *D. desulfuricans* Essex 6; *Ds*, *D. salexigens*; *Dd*, *D. desulfuricans*; *Da*, *D. africanus*; and *Dmn*, *Desulfomicrobium norvegicum*.

0006-3495/03/11/3367/08 $2.00

1993). We will generally use the originally reported sequence numbering to retain consistency with the literature. When the new numbering is required, it will be shown in italics.

We have focused our attention on Y43, and have investigated the structural and redox properties of two mutations, Y43F and Y43L. Moreover, the kinetics of reduction of Y43L cyt c_3 by 5-deazariboflavin semiquinone (5-dRfH$^{\bullet}$, $E_m = -650$ mV) were also investigated using laser flash photolysis to examine the effect of amino-acid replacement on electron transfer kinetics. The physicochemical and kinetic results obtained are discussed in the context of the three-dimensional structure of Y43L cyt c_3 at 0.91 Å resolution.

MATERIALS AND METHODS

Reagents and enzymes

Synthetic oligonucleotides were purchased from Amersham Pharmacia. Restriction endonucleases and the Mutan-Super Express Km kit used for site-directed mutagenesis were from Takara Shuzo (Kusatsu, Japan). Nucleotide sequencings of pKF19k derivative vectors were carried out using infrared dye-labeled custom primers, Forward-IRD700 (5′-ATGACCATGATTACGCCAAGCTTGC-3′) and Reverse-IRD800 (5′-GTCACGACGTTGTAAAACGACGGCC-3′) (LI-COR, Lincoln, NE), with a SequiTherm EXCEL II DNA Sequencing Kit-LC (Epicentre Technologies, Madison, WI). The [NiFe] hydrogenase was purified from the *Dv*MF crude membrane fraction according to the reported method (Yagi and Maruyama, 1971).

Site-directed mutagenesis and purification of mutant proteins

Plasmid pUCMC3, containing the gene for *Dv*MF cyt c_3 (Ozawa et al., 2001), was digested with *Pst*I and *Eco*RI, and the *Dv*MF cyt c_3 gene was ligated at the same sites of the pKF19k vector (Gene bank accession No. D63847) to generate pKFC3k. Plasmid pKFC3k containing dual-amber mutations on the gene encoding a kanamycin resistance protein was used as a template for site-directed mutagenesis. The codon for Y43 in the cyt c_3 gene in pKFC3k was replaced with that for Leu or Phe, using oligonucleotide-dual-amber-LA PCR-based mutagenesis, essentially as described by Hashimoto-Gotoh et al. (1995). Mutagenic oligonucleotides Y43L (5′-CGGCAAGGAAGATCTCCAGAAGTGCGCC-3′) and Y43F (5′-CGGCAAGGAAGATTTCCAGAAGTGCGCC-3′) were used to change the TAC codon at nucleotides 459–461 (Kitamura et al., 1993) into CTC and TTC, respectively.

The mutated genes were sequenced with a LI-COR Model 4200 DNA sequencer to confirm the presence of the desired mutations and the absence of any unwanted mutations. The mutated plasmids, pY43L and pY43F, were directly electrotransferred to *Shewanella oneidensis* TSP-C (Ozawa et al., 2001), and the recombinants were aerobically grown at 30°C in two liters of 2 × YT (with 10 mg rifampicin and 200 mg kanamycin / L) media in 3-liter Erlenmeyer flasks. The mutant cyt c_3 were purified according to the reported method (Ozawa et al., 2000). Protein mass numbers were determined by MALDI-TOF mass spectrometry using a Voyager TMDE (PerSeptive Biosystems, Framingham, MA) to confirm the mutation.

NMR and electrochemical characterization of the mutant DvMF cyt c_3

For NMR measurements, samples (1∼2 mM) were prepared as previously described (Park et al., 1996). Most ^{1}H-NMR spectra were recorded at 303 K in 30 mM sodium phosphate buffer (^2H_2O), at p^{2}H 7.0, at 400, 500, and 600 MHz with Bruker (Karlsruhe, Germany), DRX-400, DRX-500, and DRX-600 spectrometers respectively. NOESY spectra were measured with a mixing time of 15 ms, a data size of 2048 × 512, and a spectral width of 24 kHz. Chemical shifts are presented in parts per million (ppm) relative to the internal standard of 2,2-dimethyl-2-silapentane-5-sulfonate (DSS). Differential pulse polarograms were obtained with a PerkinElmer (Oak Ridge, TN) 394 digital electrochemical trace analysis system using a dropping mercury electrode. The modulation amplitude, sweep rate, and drop time were 20 mV, 4 mVs^{-1}, and 2 s, respectively. The polarograms were fitted using the analytical equation for the four consecutive one-electron reversible electrode reactions (Niki et al., 1984). Redox potentials are referred to the standard hydrogen electrode at 30°C in this work.

Laser flash photolysis experiments

Laser flash photolysis was carried out at room temperature using an N_2-dye laser (Laser photonics), which excites 5-deazariboflavin (5-dRf) to produce its semiquinone species, 5-dRfH$^{\bullet}$ ($E_m = -650$ mV) in the presence of excess EDTA (Tollin et al., 1986). Then 5-dRfH$^{\bullet}$ reduces cyt c_3. The concentrations of 5-dRf and EDTA were 60–120 μM and 10 mM, respectively. All kinetic experiments were performed under pseudo first-order conditions with a heme concentration of 2–5 μM. The buffer solution (20 mM sodium phosphate, pH 7) was placed in a rubber septum-sealed cuvette and bubbled with oxygen-depleted and water-saturated argon for 1 h to remove the residual oxygen before addition of cytochrome. The reduction of cyt c_3 by 5-dRfH$^{\bullet}$ was monitored as the intensity of the α-peak at 552 nm. Before laser flash photolysis, the cyt c_3 was partially reduced by illuminating the sample in the presence of 5-dRfH$^{\bullet}$ and EDTA, with a 35-W tungsten lamp at a distance of ∼12 cm for illumination with 1–30 s intervals. The concentration of oxidized heme was determined spectrophotometrically before each laser flash, and was checked immediately after the flash photolysis to ensure that the concentration of the oxidized heme had not changed significantly.

Crystallization and three-dimensional structure determination of wild-type and Y43L cyt c_3

Crystals of the wild-type and Y43L cyt c_3 from *Dv*MF were grown at 10°C by the vapor diffusion method. Forty to 100 μl of the protein solution, 15 mg/ml (12.5 mM Tris-HCl, pH 7.4) containing 50% (v/v) ethanol, was equilibrated against 10 ml of a buffer solution (10 mM Tris-HCl, pH 7.4) containing 60%(v/v) ethanol. Diffraction experiments were carried out at 100 K using synchrotron x-ray beams (wavelengths: 0.700 Å, Y43L; and 0.710 Å, wild-type) at the BL-44B2 beam line of SPring-8. The crystals of the wild-type and Y43L cyt c_3 belong to orthorhombic space group $P2_12_12_1$. The changes in the cell parameters between two structures were within 1%. Since the crystals diffracted to the ultrahigh resolution range, diffraction data in low ($\infty = 1.80$ Å) and high ($\infty = 0.90$ Å) resolution ranges were separately collected under different conditions, using a MAR-CCD detector system. They were processed and merged with programs MOSFLM (Leslie, 1990) and SCALA (Collaborative Computational Project, 1994), respectively. The structure refinement was started with a program package of X-PLOR (Brünger, 1992) using the atomic coordinates of the wild-type cyt c_3 at 1.8 Å resolution (Higuchi et al., 1984) without water molecules, and followed with SHELXL (Sheldrick and Schneider, 1997). All atoms including water oxygen atoms were refined with anisotropic B factors. At the final stage of the refinement, hydrogen atoms were incorporated at the calculated positions.

RESULTS

Macroscopic and microscopic redox potentials of Y43L and Y43F cyt c_3

^{1}H-NMR spectra of the wild-type, Y43L, and Y43F cyt c_3 in

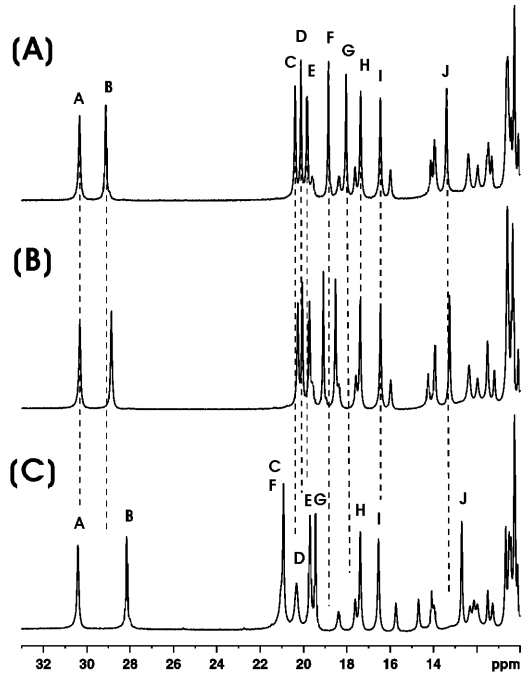

FIGURE 1 ^{1}H-NMR spectra of wild-type, Y43F, and Y43L ferricyt c_3 at 500 MHz. (*A*) Wild-type, (*B*) Y43F, and (*C*) Y43L cytochromes c_3 at 303 K. Only the fingerprint regions are presented. The heme methyl signals are labeled alphabetically (*A*–*J* in this region) from low to high field. The assignment of signals is given in Table 1.

the fully oxidized state (S_0) are shown in Fig. 1. The chemical shifts of the wild-type, Y43L and Y43F heme methyl signals are presented in Table 1. The chemical shifts of Y43F cyt c_3 are similar to those of the wild type (within a few percent, S_0), indicating that the immediate heme environment is not significantly altered by this mutation. In contrast, the Y43L mutation induced clear changes in the heme methyl signals except for those of heme 4, indicating that the substitution of leucine at position 43 affects the environment in the vicinity of hemes 1, 2, and 3. The pH dependences of the relevant signals are presented for the wild-type and Y43L cyt c_3 in Fig. 2. The features mentioned above were confirmed in a wide pH range. There are two regions where a chemical shift changes depending on pH. Although the extent of the change is different for some signals, the nature of their pH dependence is similar for the wild-type and mutant. Therefore, it can be concluded that the replacement of Y43 by Leu does not change the nature of the ionizing groups around hemes in the range from pH 5 to 10.

The stepwise reduction of Y43L and Y43F can be resolved into five ^{1}H-NMR spectra for each mutant as found for wild-type cyt c_3 (Park et al., 1996, Fan et al., 1990). The individual spectra correspond to those of the five macroscopic oxidation states: the fully-oxidized (S_0), the one-electron-reduced (S_1), the two-electron-reduced (S_2), the three-electron-reduced (S_3), and the fully-reduced (S_4) states. This observation can

TABLE 1 Chemical shifts of the heme methyl signals in the five macroscopic oxidation states of the wild-type, Y43L, and Y43F cytochromes c_3 (top, second, and bottom rows, respectively) in 30 mM phosphate buffers at p^{2}H 7.0 and 303 K

	Chemical shift in each oxidation state/ppm				
Signals	S_0 (mut-wild)*	S_1	S_2	S_3	S_4
heme 1					
B [18^1–CH$_3$]	29.31	26.97	13.06	5.05	3.30
Y43F	28.94 (−0.37)	26.26	12.59	4.80	3.24
Y43L	28.23 (−1.08)	21.02	9.27	4.19	3.69
F [2^1–CH$_3$]	18.98	17.70	9.95	4.30	2.80
Y43F	19.10 (0.12)	17.60	9.39	4.10	2.71
Y43L	21.01 (2.03)	16.16	8.02	4.78	3.20
G [12^1–CH$_3$]	18.07	17.26	9.08	3.55	2.97
Y43F	18.51 (0.44)	17.47	8.65	3.76	2.92
Y43L	19.41 (1.34)	14.61	6.45	3.43	2.90
heme 2					
C [18^1–CH$_3$]	20.51	19.83	16.37	6.70	3.15
Y43F	20.27 (−0.24)	19.67	16.75	6.76	3.12
Y43L	21.01 (0.50)	20.30	17.05	7.10	3.12
D [7^1–CH$_3$]	20.24	19.30	14.75	6.20	3.18
Y43F	20.11 (−0.13)	19.14	15.13	6.21	3.13
Y43L	20.34 (0.10)	18.68	14.60	6.35	3.10
heme 3					
E [12^1–CH$_3$]	19.90	16.88	13.46	13.02	3.49
Y43F	19.67 (−0.23)	16.95	14.03	13.58	3.43
Y43L	19.68 (−0.22)	16.37	15.09	13.00	3.42
J [2^1–CH$_3$]	13.53	13.86	11.45	11.80	4.68
Y43F	13.91 (0.38)	13.36	11.80	12.22	4.65
Y43L	14.05 (0.52)	13.05	10.25	11.90	4.63
L [7^1–CH$_3$]	10.35	8.56	[8.06]	8.60	3.99
Y43F	10.28 (−0.07)	8.79	8.14	8.68	3.95
Y43L	10.26 (−0.09)				3.94
P [18^1–CH$_3$]	−3.68	−2.21	−1.25	−0.50	3.65
Y43F	−3.74 (−0.06)	−2.31	−1.60	−0.45	3.61
Y43L	−3.74 (−0.06)	−2.17	−1.48	−0.54	3.61
heme 4					
A [18^1–CH$_3$]	30.51	12.11	10.81	7.57	3.28
Y43F	30.40 (−0.11)	11.85	9.14	6.56	3.23
Y43L	30.40 (−0.11)	19.00	12.80	7.48	3.21
H [2^1–CH$_3$]	17.53	7.60	6.77	5.45	3.63
Y43F	17.38 (−0.15)	7.84	6.45	5.20	3.62
Y43L	17.46 (−0.07)	11.41	8.22	5.62	3.57
I [12^1–CH$_3$]	16.45	7.35	6.60	5.50	3.76
Y43F	16.45 (0.00)	7.16	6.28	5.29	3.72
Y43L	16.54 (0.09)	10.95	8.11	5.73	3.69
K [7^1–CH$_3$]	10.62	6.13	5.50	5.15	3.00
Y43F	10.58 (−0.04)	6.20	5.41	4.95	2.95
Y43L	10.37 (−0.25)	7.87	6.50	5.13	2.94

S_i denotes the *i*-electron-reduced state. The data for the wild type are from Fan et al. (1990).

*The chemical-shift differences (*mutant* − *wild*) are in parentheses.

be explained by the combination of two distinct exchange rates: first, by the intermolecular electron exchange that is sufficiently slow to give rise to distinct signals for each macroscopic oxidation state; and second, by the intramolecular electron exchange between hemes within cyt c_3, which is sufficiently fast to average out the chemical shifts of each heme for the oxidized and reduced states, giving rise to

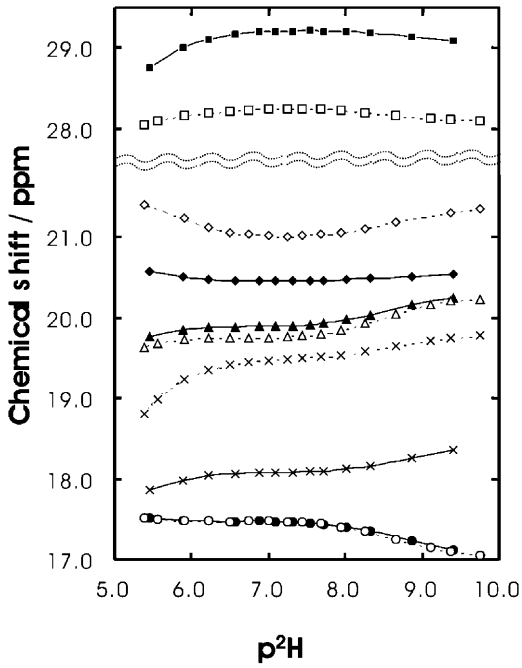

FIGURE 2 The chemical shifts of heme methyl signals as a function of p^2H at 600 MHz. Squares, diamonds, inverse triangles, crosses, and circles represent the signals *B*, *C*, *E*, *F*, and *H* (see Table 1), respectively. Solid and broken lines stand for the wild-type and Y43L cyt c_3, respectively. Temperature is 303 K.

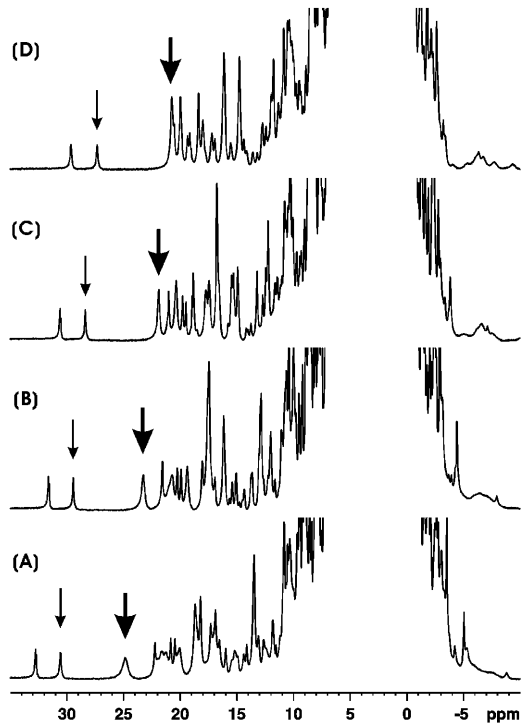

FIGURE 3 ^{1}H-NMR spectra of partially reduced Y43L cyt c_3 at 600 MHz (coexistence of S_0 and S_1) at different temperatures. (*A*) 283 K, (*B*) 293 K, (*C*) 303 K, and (*D*) 313 K. The thin and thick arrows indicate signal *B* in S_0 and S_1, respectively.

single set of signals for each heme in a certain macroscopic oxidation state. However, line-widths of the spectra of Y43L cyt c_3 in the intermediate oxidation states are broader than those of the wild type and Y43F (30–150 Hz). Since the line-width is the function of ratio of the exchange rate to the chemical shift difference in two oxidation states, either the intramolecular or the intermolecular electron exchange is affected by the Y43L mutation. In the former case, the line broadening will become more significant on lowering the temperature (that is, slowing the exchange rate), whereas the situation is the opposite in the latter case. As can be seen in Fig. 3, the line-widths of the S_1 signals become sharper with an increase in temperature (from 330 Hz at 283 K to 133 Hz at 303 K for signal *B*), suggesting that the origin of the broadening is the slower intramolecular electron transfer. This conclusion is confirmed by the observation that the spectrum for the mixture of the S_0 and S_1 states shows that the line-widths of the signals for S_1 are much broader than those for S_0 (Fig. 3), because the intermolecular exchange broadening should also appear in the signals in S_0. Line-broadenings of the heme methyl signals were reported in the intermediate oxidation states for *Dv*H cyt c_3 (Turner et al., 1996). They were attributed to the slow proton exchange because of different pK_a in different oxidation states. This is not the case for Y43L cyt c_3, because the origin of the line-broadening is the fast exchange as mentioned above.

Two-dimensional chemical exchange (NOE) spectra at 400 MHz were obtained for different intermediate redox stages to determine the chemical shifts of the heme methyl groups in the five macroscopic oxidation states. The heme proton signals in the fully reduced state (S_4) were independently assigned using TOCSY and NOESY as reported previously for wild-type cyt c_3 (Ohmura et al., 1997). The assignment of the heme methyl signals in the five macroscopic oxidation states were established on the basis of the assignment in the fully reduced state. The results for Y43L and Y43F cytochromes c_3 are summarized in Table 1. The reduction fraction (R) of each heme (the contribution to total reduction of each heme) can be obtained from the chemical shifts in Table 1 according to the equation in Table 2 (Fan et al., 1990). The average reduction fractions were calculated under the conditions of $\Sigma_i R_i^j = \Sigma_j R_i^j = 1$ using signals *B* for heme 1, *C* for heme 2, *E* for heme 3, and *H* for heme 4, following the selection of signals by Turner et al. (1996), and given in Table 2. Here, i and j stand for the heme and reduction step numbers, respectively. The data in Table 2 demonstrates that the order of reduction (major fraction at each step) is hemes 4, 1, 2, and 3, for both Y43L and Y43F cyt c_3, as has been found for the wild type (Park et al., 1996).

To determine the microscopic redox potentials, the macroscopic redox potentials of Y43L and Y43F cyt c_3

TABLE 2 The reduction fractions of the four hemes at the four reduction steps

	R^{I}	R^{II}	R^{III}	R^{IV}
Y43L				
heme 4	0.442	0.237	0.167	0.153
heme 1	0.301	0.487	0.187	0.025
heme 2	0.047	0.190	0.536	0.227
heme 3	0.210	0.086	0.109	0.594
Y43F				
heme 4	0.693	0.105	0.090	0.112
heme 1	0.104	0.536	0.302	0.058
heme 2	0.035	0.174	0.582	0.209
heme 3	0.167	0.184	0.027	0.622

The average reduction fractions were calculated by the least-squares fitting method under the conditions of $\Sigma_i R_i^j = 1$ and $\Sigma_j R_i^j = 1$, where i and j stand for the heme and reduction step numbers, respectively. Reduction fraction, $R_i^j = [\nu(S_{i-1}) - \nu(S_i)]/[\nu(S_0) - \nu(S_4)]$, where $\nu(S_i)$ is the chemical shift in oxidation state S_i.

were obtained by analyzing differential pulse polarograms, as described in Materials and Methods and are given in Table 3 along with the wild-type parameters. The microscopic redox potentials at the first and fourth reduction steps (e^{I} and e^{IV}, respectively, with the subscript representing heme number), and the interacting potentials (I_{ij} for hemes i and j) were determined using the macroscopic redox potentials and the average reduction fractions as described previously (Fan et al., 1990). The results are presented in Table 3 together with the results for the wild type. In the Y43L mutation, the changes in e_1 are relatively large (44 and 34 mV) in comparison with those in other hemes, showing that the effect of mutation is local. It led to inversion of the order of e_3^{I} and e_1^{I}. With the Y43F mutation, however, the changes are small for every heme.

TABLE 3 The macroscopic ($E_i^{0'}$ at the ith reduction step) and microscopic (e_i^{I} and e_i^{IV}, respectively) redox potentials, and the interacting potentials I_{ij}

	Potential/mV (deviation from the wild)		
	Wild type*	Y43L	Y43F
e_1^{I}	−307	−263 (+44)	−303 (+4)
e_2^{I}	−332	−312 (+20)	−330 (+2)
e_3^{I}	−287	−273 (+14)	−290 (−3)
e_4^{I}	−251	−253 (−2)	−253 (−2)
e_1^{IV}	−289	−254 (+35)	−282 (+7)
e_2^{IV}	−317	−311 (+6)	−316 (+1)
e_3^{IV}	−344	−336 (+8)	−345 (−1)
e_4^{IV}	−306	−301 (+5)	−300 (+6)
I_{12}	+40	+25 (−15)	+44 (+4)
I_{13}	−20	−12 (+8)	−27 (−7)
I_{14}	−2	−4 (−2)	+2 (+4)
I_{23}	−5	−16 (−11)	−4 (+1)
I_{24}	−20	−8 (+12)	−25 (−5)
I_{34}	−32	−36 (−4)	−24 (+8)
$E_1^{0'}$	−242	−232 (+10)	−243 (−1)
$E_2^{0'}$	−296	−271 (+25)	−293 (+3)
$E_3^{0'}$	−313	−303 (+10)	−314 (−1)
$E_4^{0'}$	−358	−350 (+8)	−357 (+1)

Subscripts in e and I denote heme numbers. The superscripts of e show the reduction steps. The error is ±2 mV.

*Recalculated from the data reported by Fan et al. (1990).

Laser flash photolysis experiments on wild-type and Y43L cyt c_3

Laser flash photolysis experiments were carried out for both the wild-type and Y43L cyt c_3 to determine if the mutation influenced the electron transfer kinetics. Although the reduction of fully oxidized cyt c_3 by 5-dRfH$^{\bullet}$ can be described with a single apparent second-order rate constant, the four hemes have been shown to have different reactivity with reductants with the wild-type cyt c_3 as reported previously (Akutsu et al., 1992). An insight into the contributions of the individual hemes to the rate constant was obtained by performing photo titration experiments involving laser flash photolysis on cyt c_3 samples that were partially reduced by white light illumination before flash photolysis. The pseudo first-order rate constant (k_{obs}) for reduction by 5-dRfH$^{\bullet}$ was plotted against the fraction of the heme reduced before the laser flash, as shown in Fig. 4. The observed curve is quite different for the wild type as

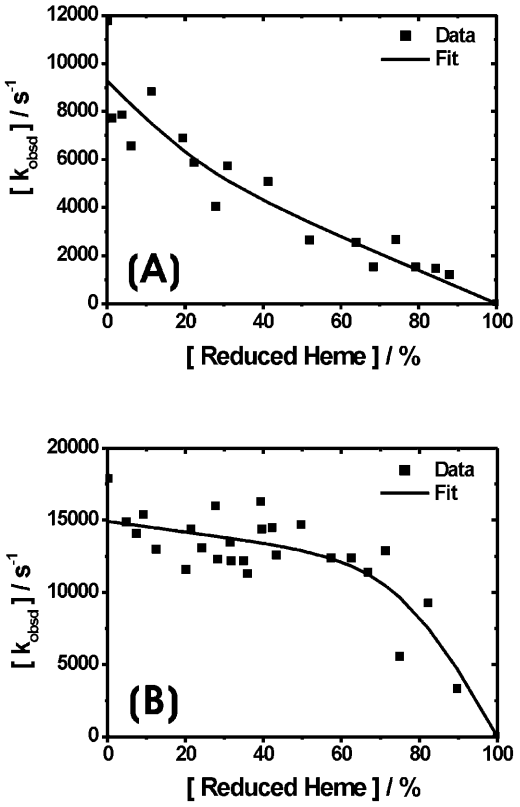

FIGURE 4 Pseudo first-order rate constants for the reduction of wild-type and Y43L cyt c_3 by 5-dRfH$^{\bullet}$ plotted as a function of %-reduced heme. (*A*) Wild-type and (*B*) Y43L cytochromes c_3. The pseudo first-order rate constants were obtained from laser flash photolysis experiments on partially reduced samples. The best-fit curves are the solid lines (see text).

compared to the Y43L mutant. To obtain information on the individual rate constant for each macroscopic oxidation form (the molecules in the S_i state), the kinetic data can be analyzed assuming that the reduction of each macroscopic oxidation form makes a contribution to the observed kinetics that depends on its rate constant and the relative amount of the heme oxidized (Akutsu et al., 1992). The concentrations of the fully oxidized, one-electron-reduced, two-electron-reduced, and three-electron-reduced forms can be estimated using the macroscopic redox potentials and the total concentrations of the oxidized hemes obtained from the absorption spectrum.

The simplest model is one in which the rate constants for all four macroscopic oxidation forms, namely, all four hemes, are identical within the limits of resolution. However, this would result in a linear plot of the observed rate constant against the fraction of the heme reduced. Clearly this is not the case (Fig. 4). The next simplest model is one where the data can be described by two rate constants; in this case, there are seven possible equations, as shown below (Akutsu et al., 1992),

$$k_{obs} = k_i([c_i] + [c_{ii}]) + k_{iii}([c_{iii}] + [c_{iv}]) \quad (1a)$$

$$k_{obs} = k_i([c_i] + [c_{iii}]) + k_{ii}([c_{ii}] + [c_{iv}]) \quad (1b)$$

$$k_{obs} = k_i([c_i] + [c_{iv}]) + k_{ii}([c_{ii}] + [c_{iii}]) \quad (1c)$$

$$k_{obs} = k_i[c_i] + k_{ii}([c_{ii}] + [c_{iii}] + [c_{iv}]) \quad (2a)$$

$$k_{obs} = k_{ii}[c_{ii}] + k_i([c_i] + [c_{iii}] + [c_{iv}]) \quad (2b)$$

$$k_{obs} = k_{iii}[c_{iii}] + k_i([c_i] + [c_{ii}] + [c_{iv}]) \quad (2c)$$

$$k_{obs} = k_{iv}[c_{iv}] + k_i([c_i] + [c_{ii}] + [c_{iii}]), \quad (2d)$$

where k_j and c_j denote the apparent second-order rate constant and the concentration of the (j-1)-electron reduced form, respectively. For Eq. 1a, for example, $k_i = k_{ii}$, whereas $k_{iii} = k_{iv}$. The data were fitted by nonlinear least-squares fitting to each equation listed above (Eqs. 1a–2d). The best fit for the reduction of the wild-type was obtained with Eq. 2a, with the fit shown as a solid line in Fig. 4 *A*. This fit (see Table 4 for the fitted rate constants) is consistent with the previous result, at a low ionic strength, using the wild-type *Dv*MF cyt c_3 (Akutsu et al., 1992). In contrast, the best fit for the reduction of Y43L cyt c_3 was obtained with Eq. 2d, and the curve obtained from the best-fit parameters is given in Fig. 4 *B*, and apparent rate constants are summarized in Table 4. Clearly, the analysis is limited by the ability to resolve individual rate constants and the use of models, which assume the minimum number of resolvable rate constants. Nevertheless, the data show a clear change in the rate constant for the fourth reduction step.

TABLE 4 Apparent second-order rate constants for reduction of wild-type and Y43L cytochromes c_3 by 5-dRfH$^{\bullet}$

	Wild type* $\times 10^{-8}$ M^{-1} s^{-1}	Y43L† $\times 10^{-8}$ M^{-1} s^{-1}
k_i	3.9 ± 0.9	1.1 ± 0.6
k_{ii}	1.6 ± 0.2	1.1 ± 0.6
k_{iii}	1.6 ± 0.2	1.1 ± 0.6
k_{iv}	1.6 ± 0.2	14.7 ± 1.1

*Rate constants derived from fitting using Eq. 2a with $k_{ii} = k_{iii} = k_{iv}$.
†Rate constants derived from fitting using Eq. 2d with $k_i = k_{ii} = k_{iii}$.

The crystal structure of wild-type and Y43L cyt c_3

The refinement of the structures of the oxidized wild-type and Y43L cyt c_3 has been completed at 1.15 (PDB code 1J0O) and 0.91 Å (PDB code 1J0P) resolution with crystallographic R-factors (free R) of 10.77 (16.69)% and 10.57 (13.60)%, respectively. The mean standard errors of the positional parameters for all protein, main-chain, and side-chain atoms were 0.019, 0.015, and 0.023 Å, respectively, for the Y43L mutant in full matrix least-squares refinement without all restraints. The mean coordinates error estimated on the basis of a Luzzati plot (Luzzati, 1952) was smaller than 0.030 Å for both structures. Eight and 17 ethanol molecules were identified in the wild-type and Y43L structures, respectively. In addition, two sulfate anions were clearly identified near Lys57 and Lys101.

The overall structures of the wild-type and Y43L cyt c_3 are almost identical. The root mean square deviation for all identical protein atoms was found to be 0.525 Å between the wild-type and Y43L structures with the program SHELX-PRO (Sheldrick and Schneider, 1997). The most striking feature of the Y43L mutant structure is the displacement of several residues in the N-terminal region in comparison with the wildtype (Fig. 5 *A*). The side-chain atom, Cδ1, of Leu43 pushes out the atoms of Ala0-Lys3 (*Ala1-Lys4*). The α-carbon atom of Ala1 (*Ala*2) is displaced by 1.1 Å. In addition, the Oε2 atom of Glu96 in the Y43L mutant was displaced by 1.1 Å. This residue is located in the vicinity of heme 2 but far from the mutated position. In the Y43L structure, the propionate groups at C-13 of heme 1 and heme 2 exist in two resolvable conformations. One of the carboxyl oxygens of the propionate group of heme 1 retains the hydrogen bond with the amide proton of Cys46 in both conformers as that found for the wildtype. The two conformers of heme 2 are shown in Fig. 5 *B*. The solvent accessibilities obtained by WHAT IF (Vriend, 1990) for hemes 1, 2, 3, and 4 of the wild type are 145, 161, 137, and 133 $Å^2$, respectively. Those of the Y43L mutant are 142 (same for two conformers), 164 and 147 (for two conformers, respectively), 130, and 142 $Å^2$, respectively.

DISCUSSION

The crystal structure of Y43L cyt c_3 showed that the mutation changes the conformation of the N-terminal peptide chain, which will affect only the environment of heme 1. In contrast, the mutation affects the nature of the axial coordination of not only heme 1 but also hemes 2 and 3, judging from the chemical shift changes of the heme methyl

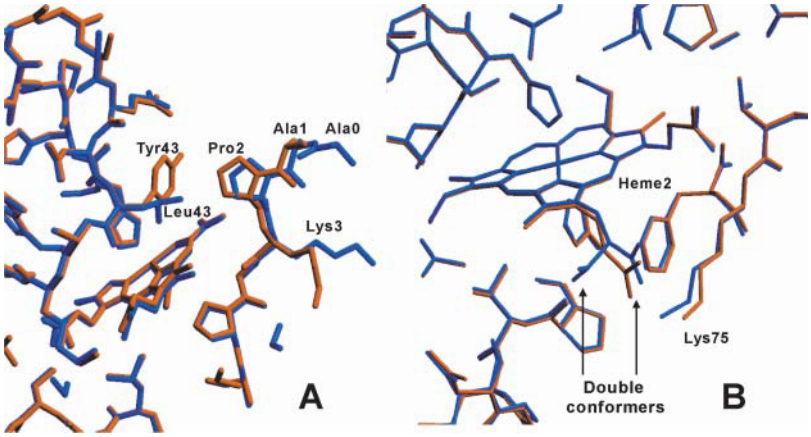

FIGURE 5 Comparison of the crystal structures of wild-type and Y43L cyt c_3. (*A*) The N-terminal region (around Pro2) of the Y43L structure is shifted from the position in the wild type. The structure models are color-coded red and blue for the wild-type and Y43L proteins, respectively. (*B*) Double conformers of the propionate group at C13 of heme 2 in the Y43L (*blue*) structure.

signals. The microscopic redox potentials in the first reduction step (e^{I}) showed a similar tendency (Table 3). This suggests that the structural perturbation at position 43 propagates from heme 1 to hemes 2 and 3 in solution.

Although Leu and Phe are both hydrophobic, only Y43L substitution induced changes in the redox potentials. Therefore, the aromaticity should be responsible for lowering the redox potentials. The effect of the aromatic ring on the redox potentials was found local. Therefore, this should not be the major reason for the extremely low redox potentials of cyt c_3. It is well-known that the bis-imidazole coordination and high exposure of the hemes are important factors to lower the redox potentials of cyt c_3. The structural element mentioned above should be another complementary factor to lower them. While the aromatic ring orients parallel to the imidazole ring of His34 in the crystal structure of the oxidized form, it moves away from the ligand in the reduced solution structure (Harada et al., 2002). The π-π interaction between the stacked rings seems to stabilize the oxidized form of heme 1. Since the main chain of Y43 is located close to heme 2, the loss of the π-π interaction should also be associated with the large decrease in the interacting potential I_{12} for the Y43L mutant. This is consistent with the previous report (Harada et al., 2002) that Tyr43 is involved in the cooperative reduction between hemes 1 and 2. Furthermore, suppression of the intramolecular electron exchange rate was found for Y43L cyt c_3, a situation not encountered with Y43F.

Laser flash photolysis of the Y43L protein provided an insight into the reduction mechanism. The apparent rate constant k_{iv} was found to be 13× greater than k_{i}, k_{ii}, and k_{iii}, which were not resolvable, and ~9× as large as k_{iv} for the wild-type cyt c_3 (Table 4). This means that the reduction rate of the three-electron-reduced form of Y43L cyt c_3 is different from those of the other macroscopic oxidation forms and also from the same oxidation form of the wild type. The heme responsible for the major reduction of this oxidation form is heme 3 (Tables 2 and 3). However, the relatively small changes in redox potential induced by Y43L mutation do not provide a reasonable explanation for the significant change in k_{iv} for Y43L relative to the other three rate constants and relative to k_{iv} for the wild type. A significant change in individual rate constants could be ascribed to a significant change in heme accessibility. However, the crystal structures determined in this work do not indicate any large changes in heme accessibility in the fully oxidized state. In contrast, the Y43L mutation results in the slower intramolecular electron transfer, and it also appears to suppress the interaction between hemes 1 and 2. This can change the reduction rate of heme 3 through intramolecular electron transfer. Consequently, the 5-dRfH$^{\bullet}$ reduction kinetics of the four hemes might not be independent processes, but instead correlated through intramolecular electron transfer.

We are grateful to Prof. G. Tollin (University of Arizona) for the kind donation of 5-deazaribflavin, to Profs. S. Aimoto and T. Kawakami (Osaka University) for measurement of mass spectra, and to Drs. Y. Shiro and S. Adachi (RIKEN Harima Inst/SPring8) for their technical advice.

This research was partly supported by grants from the Ministry of Education, Science, Technology, Sport and Culture of Japan (CREST to H.A.), and from the National Institutes of Health (GM21227 to M.A.C.).

REFERENCES

Akutsu, H., J. H. Hazzard, R. G. Bartsch, and M. A. Cusanovich. 1992. Reduction kinetics of the four hemes of cytochrome c_3 from *Desulfovibrio vulgaris* by flash photolysis. *Biochim. Biophys. Acta*. 1140:144–156.

Ambler, R. P. 1980. From Cyclotrons to Cytochromes. A. B. Robinson, and N. O. Kaplan, editors. Academic Press, London. 263–279.

Brünger, A. T. 1992. X-PLOR Vers. 3.1: A System for X-Ray Crystallography and NMR. Yale University Press, New Haven, CT.

Bruschi, M. 1994. Cytochrome c_3 (M_{r} 26,000) isolated from sulfate-reducing bacteria and its relationships to other polyheme cytochromes from *Desulfovibrio*. *Methods Enzymol*. 243:140–155.

Collaborative Computational Project, Number 4, SERC Darebury Laboratory. 1994. CCP4—a suite of programs for protein crystallography. *Acta Cryst*. D50:760–763.

Coutinho, I. B., and A. V. Xavier. 1994. Tetraheme cytochromes. *Methods Enzymol*. 243:119–140.

Czjzek, M., F. Payan, and R. Haser. 1994. Molecular and structural basis of electron transfer in tetra- and octa-heme cytochromes. *Biochimie*. 76:546–553.

Czjzek, M., F. Guerlesquin, M. Bruschi, and R. Haser. 1996. Crystal structure of a dimeric octaheme cytochrome c_3 (M(r) 26,000) from *Desulfovibrio desulfuricans norvegicum*. *Structure*. 4:395–404.

Czjzek, M., L. ElAntak, V. Zamboni, X. Molleri, A. Dolla, F. Guerlesquin, and M. Bruschi. 2002. Crystal structure of the hexadeca-heme cytochrome Hmc and structural model of its complex with cytochrome c_3. *Structure*. 10:1677–1686.

Dolla, A., L. Florens, P. Bianco, J. Haladjian, G. Voordouw, E. Forest, J. D. Wall, F. Guerlesquin, and M. Bruschi. 1994. Characterization and oxidoreduction of cytochrome c_3 after heme axial ligand replacements. *J. Biol. Chem.* 269:6340–6346.

Fan, K., H. Akutsu, Y. Kyogoku, and K. Niki. 1990. Estimation of microscopic redox potentials of a tetraheme protein, cytochrome c_3 of *Desulfovibrio vulgaris* Miyazaki F and partial assignments of heme groups. *Biochemistry*. 29:2257–2263.

Harada, E., Y. Fukuoka, T. Ohmura, A. Fukunishi, G. Kawai, T. Fujiwara, and H. Akutsu. 2002. Redox-coupled conformational alterations in cytochrome c_3 from *D. vulgaris* Miyazaki F on the basis of its reduced solution structure. *J. Mol. Biol.* 319:767–778.

Hashimoto-Gotoh, T., T. Mizuno, Y. Ogasahara, and M. Nakagawa. 1995. An oligodeoxyribonucleotide-directed dual amber method for site-directed mutagenesis. *Gene*. 152:271–275.

Higuchi, Y., M. Kusunoki, Y. Matsuura, N. Yasuoka, and M. Kakudo. 1984. Refined structure of cytochrome c_3 at 1.8 Å resolution. *J. Mol. Biol.* 172:109–139.

Kitamura, M., K. Ozawa, S. Kojima, I. Kumagai, H. Akutsu, and K. Miura. 1993. The primary structure of pre-cytochrome c_3 from *Desulfovibrio vulgaris* (Miyazaki F) as determined by nucleotide sequencing of its gene and partial amino acid sequencing. *Protein Seq. Data Anal.* 5:193–196.

Leslie, A. G. W. 1990. MOSFILM Vers. 5.41, MRC Laboratory of Molecular Biology. *In* Crystallographic Computing. Oxford University Press, Oxford, UK.

Luzzati, V. 1952. Traitement statistique des erreurs dans la determination des structures cristallines. *Acta Crystallogr*. 5:802–810.

Mathews, F. S. 1985. The structure, function and evolution of cytochromes. *Prog. Biophys. Mol. Biol*. 45:1–56.

Matias, P. M., A. V. Coelho, F. M. A. Valente, D. Plaido, J. LeGall, A. V. Xavier, I. A. C. Pereira, and M. A. Carrondo. 2002. Sulfate respiration in *Desulfovibrio vulgaris* Hildenborough: structure of the 16-heme Cytochrome *c* HmcA at 2.5 Å resolution and a view of its role in transmembrane electron transfer. *J. Biol. Chem.* 277:47907–47916.

Nørager, S., P. Legrand, L. Pieulle, C. Hatchikian, and M. Roth. 1999. Crystal structure of the oxidised and reduced acidic cytochrome c_3 from *Desulfovibrio africanus*. *J. Mol. Biol.* 290:881–902.

Niki, K., Y. Kobayashi, and H. Matsuda. 1984. Determination of macroscopic standard potentials of a molecule with a reversible *n*-consecutive one-electron transfer process. Application to a tetra-heme protein: cytochrome c_3. *J. Electroanal. Chem.* 178:333–341.

Ohmura, T., T. Inobe, K. Kano, T. Horizumi, and H. Akutsu. 1997. Unusual behavior of a heme in a tetraheme protein, cytochrome c_3 from *Desulfovibrio vulgaris* Miyazaki F, in the reduction process. *J. Electroanal. Chem.* 438:237–243.

Ozawa, K., A. I. Tsapin, K. H. Nealson, M. A. Cusanovich, and H. Akutsu. 2000. Expression of a tetraheme protein, *Desulfovibrio vulgaris* Miyazaki F cytochrome c_3, in *Shewanella oneidensis* MR-1. *Appl. Environ. Microbiol.* 66:4168–4171.

Ozawa, K., F. Yasukawa, Y. Fujiwara, and H. Akutsu. 2001. A simple, rapid, highly efficient gene expression system for multiheme cytochrome *c*. *Biosci. Biotechnol. Biochem.* 65:185–189.

Park, J.-S., T. Ohmura, K. Kano, T. Sagara, K. Niki, Y. Kyogoku, and H. Akutsu. 1996. Regulation of the redox order of four hemes by pH in cytochrome c_3 from *D. vulgaris* Miyazaki F. *Biochim. Biophys. Acta*. 1293:45–54.

Pollock, W. B. R., M. Loutfi, M. Bruschi, B. J. Rapp-Giles, J. D. Wall, and G. Voordouw. 1991. Cloning, sequencing, and expression of the gene encoding the high-molecular-weight cytochrome *c* from *Desulfovibrio vulgaris* Hildenborough. *J. Bacteriol.* 173:220–228.

Salgueiro, C. A., P. N. da Costa, D. L. Turner, A. C. Messias, W. M. A. M. van Dongen, L. M. Saraiva, and A. V. Xavier. 2001. Effect of hydrogen-bond networks in controlling reduction potentials in *Desulfovibrio vulgaris* (Hildenborough) cytochrome c_3 probed by site-specific mutagenesis. *Biochemistry*. 40:9709–9716.

Sheldrick, G. M., and T. R. Schneider. 1997. SHELXL: high-resolution refinement. *Methods Enzymol*. 277:319–343.

Tollin, G., T. E. Meyer, and M. A. Cusanovich. 1986. Elucidation of the factors which determine reaction-rate constants and biological specificity for electron-transfer proteins. *Biochim. Biophys. Acta*. 853:29–41.

Turner, D. L., C. A. Salgueiro, T. Catarino, J. LeGall, and A. V. Xavier. 1996. NMR studies of cooperativity in the tetraheme cytochrome c_3 from *Desulfovibrio vulgaris*. *Eur. J. Biochem.* 241:723–731.

Vriend, G. 1990. Quality control of protein models: directional atomic contact analysis. *J. Mol. Graph.* 8:52–56.

Yagi, T., and K. Maruyama. 1971. Purification and properties of cytochrome c_3 of *Desulfovibrio vulgaris* Miyazaki. *Biochim. Biophys. Acta*. 243:214–224.